Tri-linear representations for the Laser Interferometer Space Antenna

A Letters Journal Exploring the Frontiers of Physics

October 2022

EPL, **140** (2022) 19001
doi: 10.1209/0295-5075/ac949a

www.epljournal.org

Tri-linear representations for the Laser Interferometer Space Antenna

Fredrik Andersson, Franziska Riegger, Luigi Ferraioli, Domenico Giardini and Johan Robertsson[a]

ETH Zurich, Department of Earth Sciences - Sonneggstrasse 5, 8092 Zurich, Switzerland

received 22 June 2022; accepted in final form 23 September 2022
published online 10 October 2022

Abstract – The Laser Interferometer Space Antenna (LISA) is a space-borne observatory of gravitational waves to be launched by ESA and NASA in the 2030s. Interferometric measurements are made between three spacecraft orbiting the Sun. The measurements are dependent on the geometric information due to the relative locations between the spacecraft as well as the intrinsic parameters of the astrophysical objects that generate the gravitational waves. We show that the measurements of mildly chirping gravitational waves can be approximated by means of a tri-linear representation, where the geometric information about the location of the observed object as well as that of the spacecraft locations are separated by different factors. We discuss that for low frequencies the relative approximation error is proportional to the square of the signal's carrier frequency and illustrate this accuracy in numerical experiments. For the sake of illustration, we outline a simple algorithm for extracting parameters from the observed gravitational waves.

Introduction. – For centuries, electromagnetic radiation has been the only option to observe the Universe. However, most of it remains electromagnetically dark. Instead, detection of yet unrevealed astrophysical objects and mechanisms can be achieved through Gravitational Wave (GW) observation [1,2]. These waves interact only weakly with matter and hence, travel through the Universe without distortion of the information they carry about their origins. For instance, insights into the Milky Way and galaxy formation, in general, can be obtained by analyzing measurements of GWs that are emitted by massive black holes or ultra-compact binaries [3–7].

Similar to electromagnetic waves, GWs have two polarization components. Their particular effect on the spacetime fabric is a tidal deformation. Its strength is given as the relative change in the initial extent of the matter that is distorted by the GW. For waves from astrophysical sources, this ratio typically ranges in the order of magnitude of 10^{-21}. Such small amplitudes can be detected by means of laser interferometry [1,8–13]. Since the first detector of this kind went into operation in 2002, a whole network of ground-based interferometers evolved [14–17]. In spite of the many successes, including the first direct detection of a GW in 2015 [8], terrestrial GW detection is limited: seismic noise as well as noise originating from Earth's local gravity restrict the sensitivity of ground-based interferometers to GWs that are emitted at frequencies above a few Hz [18,19]. However, it is expected that the richest part of the gravitational radiation spectrum corresponds to frequencies below 100 mHz [1]. Access to this low-frequency regime is expected to be provided by LISA, a project that is jointly proposed by ESA, NASA, and an international group of scientists, the LISA consortium [1,2]. LISA is planned to be the space-based counterpart to the terrestrial interferometric GW detectors and is designed to simultaneously detect several thousand GWs from the low-frequency regime. It consists of three spacecraft that are separated by order of millions of kilometers and arranged in a triangular formation. Laser beams are relayed back and forth between the satellites, building the interferometric arms along which the relative change due to GWs is measured. Further, LISA trails the Earth around the Sun while the spacecraft rotate around their barycenter. This orbital motion introduces

[a] E-mail johan.robertsson@erdw.ethz.ch (corresponding author)

amplitude, frequency, and phase modulations to the measured data which encodes relevant information about the gravitational wave source such as source location, orientation, and the orbital plane [6,20]. The full potential of the LISA measurements is to be exploited with data analysis algorithms that are capable of extracting individual signals from a data stream that contains an unknown number of overlapping signals [21,22]. Most of the initial attempts at LISA data analysis originate from the ground-based detector community, where the established analysis method is grid-based matched filtering [23–27]. Other statistical methods for the detection of gravitational waves have been suggested in [21,28–37].

In this paper, we propose to approach the LISA data analysis from a different direction. We show that mildly chirping gravitational waves that will be detected by LISA can be well approximated using a tri-linear structure. We will employ some rudimentary assumptions on the arm-lengths [38] and filtering in the Fourier domain [30] as also used elsewhere. The tri-linear approximation allows for a representation where contributions caused by the geometry of LISA are separated from those of the observed astrophysical object. Specifically, it is shown that the contributions of the astrophysical object further factor into: the waveform, its direction of propagation, and a term that encodes a sequence of Euler rotations together with the source's extrinsic parameters. This approximation can be used to design new detection algorithms based on linear algebra techniques. We illustrate this with a simple method using alternating least squares for an isolated event. The construction of more complex strategies falls out of the scope of this letter.

Tri-linear representations. – The gravitational wave emitted from a source in the direction $\mathsf{k} \in \mathbb{R}^3$ at a position $\mathsf{x} \in \mathbb{R}^3$ can be modeled by the tensor-valued function $\mathsf{H}_0^{\boldsymbol{\alpha}} : \mathbb{R} \times \mathbb{R}^3 \to \mathbb{R}^{3\times 3}$. The parameters describing the source are gathered in the vector $\boldsymbol{\alpha} = \{\mathsf{k}, \dots\}$, where the notation "..." indicates additional parameters. Specifically, transverse, traceless plane gravitational waves will be considered, for which the gravitational waves take the form

$$\mathsf{H}_0^{\boldsymbol{\alpha}}(t, \mathsf{x}) = \mathsf{H}^{\boldsymbol{\alpha}}(t - \mathsf{x} \cdot \mathsf{k}), \tag{1}$$

where $\mathsf{H}^{\boldsymbol{\alpha}} : \mathbb{R} \to \mathbb{R}^{3\times 3}$. This function may further be decomposed as

$$\mathsf{H}^{\boldsymbol{\alpha}}(t) = h_+^{\boldsymbol{\alpha}}(t)\mathsf{E}_+ + h_\times^{\boldsymbol{\alpha}}(t)\mathsf{E}_\times,$$

where $h_+, h_\times : \mathbb{R} \to \mathbb{R}$ represent the two polarization components. Whereas both the direction k and the polarization components strictly speaking depend on the location x, the distances to the sources of the gravitational waves and the observation points are that large so that this dependence is negligible. These quantities are therefore regarded to be constants. The polarization tensors E_+ and $\mathsf{E}_\times$ are 3×3 symmetric matrices satisfying

$$\begin{aligned} \mathsf{k}^T\mathsf{E}_+\mathsf{k} = 0, \qquad & \mathsf{k}^T\mathsf{E}_\times\mathsf{k} = 0, \\ \operatorname{trace}(\mathsf{E}_+) = 0, \qquad & \operatorname{trace}(\mathsf{E}_\times) = 0, \end{aligned} \tag{2}$$

where trace denotes the matrix trace. The elements of these matrices are included in the parameter vector $\boldsymbol{\alpha}$. We will assume that the polarization components in turn can be written as

$$h_+^{\boldsymbol{\alpha}}(t) = \operatorname{Re}\left(c_+ h^{\boldsymbol{\alpha}}(t)\right), \quad h_\times^{\boldsymbol{\alpha}}(t) = \operatorname{Re}\left(c_\times h^{\boldsymbol{\alpha}}(t)\right),$$

where $c_+, c_\times \in \mathbb{C}$ are constant amplitudes and $h^{\boldsymbol{\alpha}}$ is complex valued. This property holds true, for instance for galactic and massive black holes binaries. As will be described later on, the approach that we will present holds in the more general case, but simplifies in the above setting. We now define

$$\mathsf{E} = c_+\mathsf{E}_+ + c_\times\mathsf{E}_\times.$$

Note that it holds that $\mathsf{k}^T\mathsf{E}\mathsf{k} = 0$, and that $\operatorname{trace}(\mathsf{E}) = 0$, similarly as before. The gravitational waves that we consider can thus be described by

$$\mathsf{H}^{\boldsymbol{\alpha}}(t) = \operatorname{Re}\left(h^{\boldsymbol{\alpha}}(t)\mathsf{E}\right),$$

where $\boldsymbol{\alpha} = \{\mathsf{k}, \mathsf{E}, \dots\}$, and where the additional parameters indicated by ... describe the waveform $h^{\boldsymbol{\alpha}}$. The introduced gravitational wave model is based on [39,40] to which we refer for further information. With LISA, measurements will be made using three spacecraft, measuring fluctuations in their relative positions as a function of time by means of laser interferometers. We denote their locations by the functions $\mathsf{p}_j^0(t)$, $j \in \{1, 2, 3\}$. Moreover, we introduce

$$\mathsf{p}^0(t) = (\mathsf{p}_1^0(t) + \mathsf{p}_2^0(t) + \mathsf{p}_3^0(t))/3$$

to denote the average location, and

$$\mathsf{p}_j(t) = \mathsf{p}_j^0(t) - \mathsf{p}^0(t)$$

as the locations relative to the average location. For the moment, let us assume that

$$\mathsf{p}^0(t) = \mathbf{0}. \tag{3}$$

We also introduce the normalized direction vectors

$$\mathsf{n}_{j_1,j_2}(t) = \frac{\mathsf{p}_{j_2}(t) - \mathsf{p}_{j_1}(t)}{\|\mathsf{p}_{j_2}(t) - \mathsf{p}_{j_1}(t)\|}, \tag{4}$$

and the arm-lengths

$$L_{j_1,j_2}(t) = \|\mathsf{p}_{j_1}(t) - \mathsf{p}_{j_2}(t)\|, \quad j_1, j_2 \in \{1, 2, 3\}. \tag{5}$$

The time it takes the light to travel between two spacecrafts is often taken into account when defining the arm-lengths. In this case it is necessary to distinguish between $L_{j_1,j_2}(t)$ and $L_{j_2,j_1}(t)$. However, for the frequency range

and given the kind of approximations that we will consider in this work, this effect is marginal and it will be ignored. Moreover, we will assume that the change in positions is small compared to the time it takes for light to travel between spacecrafts. We introduce the time delay operator

$$T_\tau f(t) = f(t-\tau).$$

Regarding the remark above and using units where the speed of light is one, we will now make approximate expressions of the form

$$\begin{aligned} T_{L_{j_3,j_4}(t)} T_{L_{j_1,j_2}(t)} f(t) &= T_{L_{j_3,j_4}(t)} f(t - L_{j_1,j_2}(t)) \\ &\approx f(t - L_{j_1,j_2}(t) - L_{j_3,j_4}(t)), \end{aligned}$$

without explicitly mentioning its effect since it is negligible. Following [41,42], the response $y^{\alpha}_{1,2}$ for the one-way Doppler measurements conducted in the LISA setup (sending from spacecraft 1 and receiving at spacecraft 2) is given by

$$\begin{aligned} y^{\boldsymbol{\alpha}}_{1,2}(t) = \frac{1}{2} \frac{\mathsf{n}^T_{1,2}(t) \mathsf{E} \mathsf{n}_{1,2}(t)}{1 - \mathsf{n}_{1,2}(t) \cdot \mathsf{k}} \\ \times \Big(h^{\boldsymbol{\alpha}}(t - L_{1,2}(t) - \mathsf{p}_1(t) \cdot \mathsf{k}) - h^{\boldsymbol{\alpha}}(t - \mathsf{p}_2(t) \cdot \mathsf{k}) \Big). \end{aligned} \tag{6}$$

We will now assume that $h^{\boldsymbol{\alpha}}$ can be decomposed as

$$h^{\boldsymbol{\alpha}}(t) = g^{\boldsymbol{\alpha}}(t) \phi(t), \quad \phi(t) = e^{2\pi i \omega_0 t}, \tag{7}$$

with $g^{\boldsymbol{\alpha}}$ varying slowly in comparison to the carrying frequency ω_0. This assumption holds true for instance for the case of mildly chirping galactic binaries, and for monochromatic galactic binaries, in particular, it is possible to choose ω_0 so that $g^{\boldsymbol{\alpha}}$ becomes constant.

This representation can be made slightly more general by inluding a "carrier" chirp component, $\dot{\omega}_0$ in $\phi(t)$. Doing so allows for the representation of moderately chirping events, some more details are provided, cf. (15). However, in this letter we focus on the case above as it allows for a simpler partitioning of the frequency domain that is more useful when searching for large numbers of galactic binaries.

The right-hand side of (6) can then be approximated by

$$\begin{aligned} \frac{1}{2} \frac{\mathsf{n}^T_{1,2}(t) \mathsf{E} \mathsf{n}_{1,2}(t)}{1 - \mathsf{n}_{1,2}(t) \cdot \mathsf{k}} g^{\boldsymbol{\alpha}}(t) \phi(t) \\ \times \Big(e^{-2\pi i \omega_0 (L_{1,2}(t) + \mathsf{p}_1(t) \cdot \mathsf{k})} - e^{-2\pi i \omega_0 \mathsf{p}_2(t) \cdot \mathsf{k}} \Big), \end{aligned}$$

which we can rewrite as

$$\begin{aligned} \frac{1}{2} \frac{\mathsf{n}^T_{1,2}(t) \mathsf{E} \mathsf{n}_{1,2}(t)}{1 - \mathsf{n}_{1,2}(t) \cdot \mathsf{k}} g^{\boldsymbol{\alpha}}(t) \phi(t) e^{-2\pi i \omega_0 \mathsf{p}_2(t) \cdot \mathsf{k}} \\ \times \Big(e^{-2\pi i \omega_0 L_{1,2}(t) (1 - \mathsf{n}_{1,2}(t) \cdot \mathsf{k})} - 1 \Big). \end{aligned}$$

Let us introduce

$$\beta_{j_1,j_2}(t) = -2\pi i \omega_0 L_{j_1,j_2}(t). \tag{8}$$

In the following, let us assume that $|\beta_{j_1,j_2}(t)|$, *i.e.*, $|\omega_0 L_{j_1,j_2}(t)|$ is small. Through a series expansion we thus have that

$$\begin{aligned} y^{\boldsymbol{\alpha}}_{1,2}(t) \overline{\phi(t)} \approx \frac{1}{2} g^{\boldsymbol{\alpha}}(t) \mathsf{n}^T_{1,2}(t) \mathsf{E} \mathsf{n}_{1,2}(t) e^{-2\pi i \omega_0 \mathsf{p}_2(t) \cdot \mathsf{k}} \\ \times \Big(\beta_{1,2}(t) + \frac{1}{2!} \beta_{1,2}(t)^2 (1 - \mathsf{n}_{1,2}(t) \cdot \mathsf{k}) \\ + \frac{1}{3!} \beta_{1,2}(t)^3 (1 - \mathsf{n}_{1,2}(t) \cdot \mathsf{k})^2 + \dots \Big). \end{aligned} \tag{9}$$

Before going into further details about this expansion, let us discuss how to apply the same technique to so-called Time-Delay Interferometry (TDI) observables [41,43,44]. These are linear combinations of time delayed Doppler measurements which feature multiple beneficial characteristics. Each combination has different properties, two such being the suppression of comparatively large noise components or an increased robustness of the mission in cases where one pair of spacecraft is lost [41]. A variety of different TDI combinations exist: the first generation of unequal arm Michelson TDIs, for instance, is given by

$$\begin{aligned} X^{\boldsymbol{\alpha}}_1(t) = \big(T_{L_{1,2} y^{\boldsymbol{\alpha}}_{12}}(t) + y^{\boldsymbol{\alpha}}_{21}(t) \big) \Big(T^2_{L_{1,3}} - 1 \Big) \\ + \big(T_{L_{1,3} y^{\boldsymbol{\alpha}}_{13}}(t) + y^{\boldsymbol{\alpha}}_{31}(t) \big) \Big(T^2_{L_{1,2}} - 1 \Big), \end{aligned}$$

where $X^{\boldsymbol{\alpha}}_2(t)$ and $X^{\boldsymbol{\alpha}}_3(t)$ are obtained from cyclic permutation of indices [45]. Further combinations exist where expressions of the type $\big(T_{L_{1,2} y^{\boldsymbol{\alpha}}_{1,2}}(t) + y^{\boldsymbol{\alpha}}_{2,1}(t) \big) \overline{\phi(t)}$ appear [43]. According to the assumption that $g^{\boldsymbol{\alpha}}(t)$ is varying slowly in comparison to $\phi(t)$, cf. (7), and that this also holds true when comparing the variation in arm-length and position vectors to $\phi(t)$, we may approximate

$$T_{L_{1,2}} y^{\boldsymbol{\alpha}}_{1,2}(t) \approx e^{\beta_{1,2}(t)} y^{\boldsymbol{\alpha}}_{1,2}(t).$$

Using (9) along with similar manipulations for $y^{\boldsymbol{\alpha}}_{2,1}(t)$, along with Taylor expansions of $e^{\beta_{1,2}(t)}$ and $e^{-2\pi i \omega_0 \mathsf{p}_2(t) \cdot \mathsf{k}}$ and some calculations one obtains

$$\begin{aligned} \big(T_{L_{1,2}} y^{\boldsymbol{\alpha}}_{1,2}(t) + y^{\boldsymbol{\alpha}}_{2,1}(t) \big) \overline{\phi(t)} = \frac{1}{2} g^{\boldsymbol{\alpha}}(t) \mathsf{n}^T_{1,2}(t) \mathsf{E} \mathsf{n}_{1,2}(t) \\ \times \Bigg(\beta_{1,2}(t) \Big(2 + 2\beta_{1,2}(t) + \frac{4}{3} \beta_{1,2}(t)^2 - \beta_{1,2}(t) \frac{\mathsf{p_3(t)} \cdot \mathsf{k}}{L_{1,2}} \\ \times \big(1 + \beta_{1,2}(t) \big) + \frac{1}{3} \frac{\beta_{1,2}(t)^2}{L^2_{1,2}} \times \big((\mathsf{p_1(t)} \cdot \mathsf{k})^2 \\ + (\mathsf{p_1(t)} \cdot \mathsf{k})(\mathsf{p_2(t)} \cdot \mathsf{k}) + (\mathsf{p_2(t)} \cdot \mathsf{k})^2 \big) + \mathcal{O}\big(\beta_{1,2}(t)^3 \big) \Big) \Bigg). \end{aligned} \tag{10}$$

By dropping the quadratic dependence on k, we obtain

$$\begin{aligned} \begin{pmatrix} e^{\beta_{1,2}(t)} y^{\boldsymbol{\alpha}}_{1,2}(t) + y^{\boldsymbol{\alpha}}_{2,1}(t) \\ e^{\beta_{1,3}(t)} y^{\boldsymbol{\alpha}}_{1,3}(t) + y^{\boldsymbol{\alpha}}_{3,1}(t) \\ e^{\beta_{2,3}(t)} y^{\boldsymbol{\alpha}}_{2,3}(t) + y^{\boldsymbol{\alpha}}_{3,2}(t) \end{pmatrix} \overline{\phi(t)} \approx \\ \frac{1}{2} g^{\boldsymbol{\alpha}}(t) \begin{pmatrix} \mathsf{n}^T_{1,2}(t) \mathsf{E} \mathsf{n}_{1,2}(t) \, (a_{1,2}(t) + \mathsf{a}_3(t) \cdot \mathsf{k}) \\ \mathsf{n}^T_{1,3}(t) \mathsf{E} \mathsf{n}_{1,3}(t) \, (a_{1,3}(t) + \mathsf{a}_2(t) \cdot \mathsf{k}) \\ \mathsf{n}^T_{2,3}(t) \mathsf{E} \mathsf{n}_{2,3}(t) \, (a_{2,3}(t) + \mathsf{a}_1(t) \cdot \mathsf{k}) \end{pmatrix}, \end{aligned} \tag{11}$$

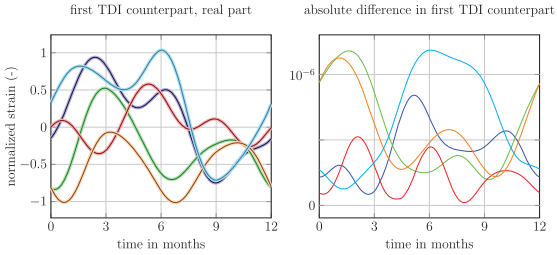

Fig. 1: Comparison between the tri-linear approximation and the reference data model. Left: the real part of $W(t,1)$ is plotted for five simulated signals (thin line, reference model; thick line, tri-linear approximation). Right: the absolute difference in these signals is depicted.

where

$$\begin{aligned} a_{1,2}(t) &= 2\beta_{1,2}(t)\left(1+\beta_{1,2}(t)+\frac{2}{3}\beta_{1,2}(t)^2\right), \\ \mathsf{a}_3(t) &= -\beta_{1,2}(t)^2\frac{\mathsf{p}_3(t)}{L_{1,2}}\Big(1+\beta_{1,2}(t)\Big), \end{aligned} \tag{12}$$

and like-wise for the other indices. This approximation is $\mathcal{O}(\beta_{1,2}(t)^4)$. We note that (11) is a tri-linear expression in $g^{\boldsymbol{\alpha}}(t)$, E, and the affine compensated vector $(1,\mathsf{k}_1,\mathsf{k}_2,\mathsf{k}_3)$. All other expressions in (11) are known and only dependent on the geometry of the spacecraft. Geometric information about the source of the gravitational wave is contained in k and E, respectively, while the information of the actual waveform is contained in $g^{\boldsymbol{\alpha}}(t)$.

Finally, let us loosen the requirement (3). From (1) we see that a change in location modifies the gravitational waves by translations of the form $\mathsf{p}^0(t)\cdot\mathsf{k}$. Hence, the counterpart of (11) in the case where (3) does not hold is

$$\begin{pmatrix} e^{\beta_{1,2}(t)}y^{\boldsymbol{\alpha}}_{1,2}(t)+y^{\boldsymbol{\alpha}}_{2,1}(t) \\ e^{\beta_{1,3}(t)}y^{\boldsymbol{\alpha}}_{1,3}(t)+y^{\boldsymbol{\alpha}}_{3,1}(t) \\ e^{\beta_{2,3}(t)}y^{\boldsymbol{\alpha}}_{2,3}(t)+y^{\boldsymbol{\alpha}}_{3,2}(t) \end{pmatrix} \approx$$

$$\frac{1}{2}h^{\boldsymbol{\alpha}}(t-\mathsf{p}^0(t)\cdot\mathsf{k})\begin{pmatrix} \mathsf{n}^T_{1,2}(t)\mathsf{E}\mathsf{n}_{1,2}(t)\,(a(t)+\mathsf{a}_3(t)\cdot\mathsf{k}) \\ \mathsf{n}^T_{1,3}(t)\mathsf{E}\mathsf{n}_{1,3}(t)\,(a(t)+\mathsf{a}_2(t)\cdot\mathsf{k}) \\ \mathsf{n}^T_{2,3}(t)\mathsf{E}\mathsf{n}_{2,3}(t)\,(a(t)+\mathsf{a}_1(t)\cdot\mathsf{k}) \end{pmatrix}. \tag{13}$$

This expression still has the structure of a matrix of rank three. As a consequence, it is easy to define a three-dimensional array with elements only depending on the geometry and the frequency ω_0. To clarify the structure further, we introduce some additional notation. We let e denote a complex vector with 5 elements such that

$$\mathsf{E}=\begin{pmatrix} \mathsf{e}_1 & \mathsf{e}_2 & \mathsf{e}_3 \\ \mathsf{e}_2 & \mathsf{e}_4 & \mathsf{e}_5 \\ \mathsf{e}_3 & \mathsf{e}_5 & -\mathsf{e}_1-\mathsf{e}_4 \end{pmatrix}.$$

This assures that $\mathrm{trace}(\mathsf{E})=\mathsf{e}_1+\mathsf{e}_4+(-\mathsf{e}_1-\mathsf{e}_4)=0$. Moreover, let $\tilde{\mathsf{k}}=(1,\mathsf{k}_1,\mathsf{k}_2,\mathsf{k}_3)$, gather the TDI-like observables in W, and introduce the four-dimensional array A so that the counterpart of (16) can be expressed as

$$W(t,j_2)\approx\sum_{j_3=1}^{5}\sum_{j_4=1}^{4}h^{\boldsymbol{\alpha}}(t-\mathsf{p}^0(t)\cdot\mathsf{k})\mathsf{A}(t,j_2,j_3,j_4)\mathsf{e}_{j_3}\tilde{\mathsf{k}}_{j_4}. \tag{14}$$

We can now easily model several sources using the same structure. We extend the vectors e and $\tilde{\mathsf{k}}$ to be two-dimensional, with the second dimension referring to the source the parameters belong to. An approximate model for M sources then reads as

$$W(t,j_2)\approx \sum_{m=1}^{M}\sum_{j_3=1}^{5}\sum_{j_4=1}^{4}h^{\boldsymbol{\alpha}_m}(t-\mathsf{p}^0(t)\cdot\mathsf{k}_{\cdot,m})\mathsf{A}(t,j_2,j_3,j_4)\mathsf{e}_{j_3,m}\tilde{\mathsf{k}}_{j_4,m}.$$

As shown in fig. 1, the accuracy of the approximation is assessed by comparison to a reference using the data model in [39]. Throughout the following comparisons, the Solar-system–baricentric coordinate system is employed and the orbits of the spacecraft are modeled up to second order in the eccentricity. The coordinates are given by eqs. (A1) and (A2) in [39] with $\eta_0=0$ and $\xi_0=0$. Arm-lengths and unit normal vectors are computed according to (4) and (5). For the comparison in fig. 1, we assume that the GWs are emitted by non-chirping galactic binaries, *i.e.*, a monochromatic signal is assumed. Sky locations and polarizations are generated randomly while their inclinations, the initial phase as well as the deviation of the frequency are set to zero and the amplitudes are chosen to be one. All depicted GWs have the same frequency ω which equals the carrier frequency $\omega_0=10^{-4}$ Hz. Each signal shown in fig. 1 is simulated for the duration of 1 year. In order to compare the real-valued LISA measurements to the complex-valued data generated by the tri-linear approximation, we compute the complex-valued analytic part of the reference signal, cf. [46], eq. 4.69. Further we eliminate the oscillation originating from ω_0 for each GW signal by multiplication with $\overline{\phi(t)}$, cf. (7). This results in the slowly oscillating signals that are depicted in fig. 1. The variations are caused by LISA's orbital motion. In fig. 2 the error between the tri-linear approximation and the reference model is depicted for different carrier frequencies ω_0. The reference and approximation are computed as above. For each ω_0, the residual is computed for 1000 different sky locations and polarizations, *i.e.*, k and e. Figure 2 illustrates the behavior of the approximation errors. For signals with the same carrier frequency, the errors exhibit mild variation. The error mainly depends on ω_0 while impacts of different choices of k and e are negligible.

Since $\beta_{j_1,j_2}\sim\omega_0$ according to (8), it follows from (10) and (11) that for small ω_0 the amplitude of the tri-linear approximation should be proportional to ω_0^3. At the same time, from (12) the amplitude of the TDI counterparts $\{W(t,j_2)\}_{j_2=1}^3$ should be proportional to ω_0. Hence, the relative errors are expected to be proportional to ω_0^2 for

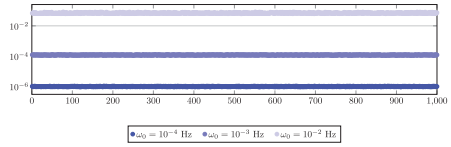

Fig. 2: Relative approximation error for three different ω_0 each having 1000 modeled signals. The parameters are assumed to be constant apart from the sky locations and polarization which are generated randomly.

low frequencies, as illustrated in fig. 2. Comparing the approximation errors to the LISA noise characteristics puts the accuracy of the tri-linear representation into perspective. The LISA Data Challenge 1-3 data set [47] contains ten verification binaries that are superimposed with the frequency-dependent instrumental LISA noise. In the close vicinity of each verification binary, the noise is at least 10% and the tri-linear representations are therefore well suited for the parameter estimation.

Tri-linear representations similar to (14) can further be derived for signals with more significant frequency derivatives. In this case, a carrier chirp $\dot{\omega}_0$ is included in $\phi(t)$ and $\beta_{j_1,j_2}(t)$ is defined as

$$\beta_{j_1,j_2}(t) = -2\pi i\omega_0 L_{j_1,j_2}(t) - 2\pi i\dot{\omega}_0 L_{j_1,j_2}(t). \tag{15}$$

The accuracy of the corresponding tri-linear structures is sufficiently low for chirps up to 10^{-12} Hz^2. This allows for instance to approximate GWs that are emitted by an equal-mass massive black hole binary with a total mass of 10^4 Solar masses and frequencies smaller than 0.5 mHz [22].

Alternating least squares for single events. – Let us consider the case where the data consist of a single event. This will of course also be relevant where parts of the data can be isolated so that they mainly contain contributions from a single event. In this scenario, we do not impose any additional constraints on the structure of the waveform $h^{\boldsymbol{\alpha}}$, except that (14) is valid. Note that if two out of the three sets of parameters $\tilde{\mathsf{k}}$, e and $h^{\boldsymbol{\alpha}}$ are fixed, then the third one can be solved by the linear system defined by (14). A strategy for finding all parameters is thus to iteratively lock two sets of parameters and update the third. This general approach is well known in the literature and often referred to as alternating least squares [48]. Amongst other use-cases it is often applied for tensor decompositions [49], numerical simulations in higher dimensions [50] but also for matrix factorizations in the case of incomplete data [51].

Let us set $f(t) = h^{\boldsymbol{\alpha}}(t - \mathsf{p}^0 \cdot \mathsf{k})$ in the description that follows. For fixed e and $\tilde{\mathsf{k}}$ the best approximation of f is obtained from minimizing the least squares problem associated with (14) for each point in time. Note that the problem is defined such that all TDI channels are used, and for the considered noise-free scenario no further constraints on the waveforms are imposed. In a similar fashion, we can obtain an initial candidate for an update of e by minimizing the least squares problem (14) obtained by fixing f and k. The corresponding matrix

$$\tilde{\mathsf{E}} = \begin{pmatrix} \tilde{\mathsf{e}}_1 & \tilde{\mathsf{e}}_2 & \tilde{\mathsf{e}}_3 \\ \tilde{\mathsf{e}}_2 & \tilde{\mathsf{e}}_4 & \tilde{\mathsf{e}}_5 \\ \tilde{\mathsf{e}}_3 & \tilde{\mathsf{e}}_5 & -\tilde{\mathsf{e}}_1 - \tilde{\mathsf{e}}_4 \end{pmatrix}$$

is not necessarily of the desired form though, as it typically would not be possible to decompose it using E_+ and $\mathsf{E}_\times$ such that (2) is satisfied. A particular problem is that $\tilde{\mathsf{E}}$ does not necessarily have one eigenvector with the corresponding eigenvalue that is, or is close to zero, *i.e.*, $\mathsf{k}^T\tilde{\mathsf{E}}\mathsf{k} = 0$ is not necessarily satisfied. Moreover, the eigenvector corresponding to the eigenvalue with the smallest absolute value is not necessarily real. This induces complications in the estimation of $\tilde{\mathsf{k}}$ which we want to be real-valued. By forming the singular value representation

$$\mathsf{U}\Sigma\mathsf{V}^{\mathsf{T}} = \begin{pmatrix} \mathrm{Re}(\tilde{\mathsf{E}}) \\ \mathrm{Im}(\tilde{\mathsf{E}}) \end{pmatrix}, \tag{16}$$

we can construct

$$\mathsf{E}_{P,i,j} = \sum_{r=1}^{2} \mathsf{U}_{i,r}\Sigma_{r,r}\mathsf{V}_{j,r} + i\,\mathsf{U}_{i+3,\mathrm{r}}\Sigma_{r,r}\mathsf{V}_{j,r} \tag{17}$$

which is an approximation of $\tilde{\mathsf{E}}$ that satisfies (2) up to the traceless condition. We may now proceed by projecting E_P on the set of traceless matrices and using that to update e. After this last projection, the constraints (2) will again not be satisfied. We thus either continue with additional iterations of the same type to improve the estimation of e, or continue with updating the estimates of $\tilde{\mathsf{k}}$ and $f(t)$. This is also a type of alternating projection method. For results regarding convergence for this class of problems see [52]. The final step concerns the estimation of $\tilde{\mathsf{k}}$ given fixed f and e. This is done by minimizing (14) via least squares. However, it is advantageous to also incorporate the constraint that $\mathsf{k}^T\mathsf{E}\mathsf{k} = 0$. This can be done by minimizing

$$\sum_{j_2=1}^{3} \int \left| W(t, j_2) - \sum_{j_3=1}^{5}\sum_{j_4=1}^{4} f(t)\mathsf{A}(t, j_2, j_3, j_4)\mathsf{e}_{j_3}\tilde{\mathsf{k}}_{j_4} \right| \mathrm{d}t + S\left(\left| \sum_{n=1}^{3} \tilde{\mathsf{k}}_{n+1}\mathsf{V}_{n,1} \right|^2 + \left| \sum_{n=1}^{3} \tilde{\mathsf{k}}_{n+1}\mathsf{V}_{n,2} \right|^2 \right), \tag{18}$$

where V are obtained from (16), and where S is some penalty level, for instance proportional to the equivalent of the Frobenious norm of A. We collect the steps above in Algorithm 1.

Figure 3 illustrates the result of the proposed alternating least squares algorithm (algorithm 1) as applied to 1000 simulations. The parameters for each simulation are chosen as described above but with

$$h^{\boldsymbol{\alpha}}(t) = e^{2\pi i\left((\omega_0+\delta\omega)t+\nu t^2/(2t^2_{\mathrm{max}})\right)}.$$

Algorithm 1: Alternating least squares for general single event.

Initialize random k, and let $f(t) = e^{-2\pi i\omega_0 \mathsf{p}^0(t)\cdot\mathsf{k}}$;
repeat{
  Compute $\tilde{\mathsf{e}}$ by minimizing the residual for (14) with fixed f and $\tilde{\mathsf{k}}$;
  Obtain e and V by (16) and (17);
  Compute $\tilde{\mathsf{k}}$ by minimizing (18);
  Compute f by least squares minimization of (14);
}**until***(Criterium reached)*

Here, $\omega_0 = 1$ mHz and both $\delta\omega$ and ν are uniformly distributed on the interval $[-1, 1] \cdot 10^{-6}$. The outcome from algorithm 1 may depend on the initial guess. As a way to illustrate this, we choose an accuracy level of 0.001 and run Algorithm 1 either until the tolerance level is reached, or a maximum value of iterations (100) is reached. When converging, the number of needed iterations is typically about 15. Note that as long as the chosen accuracy level is above the approximation error, further lowering it affects the number of iterations that are required before convergence. Reducing the tolerance level to 10^{-4}, for instance, increases the number of iteration to around 20. If convergence is not reached, the procedure is restarted using a different randomly initialized direction k. The left panel of fig. 3 depicts the relative error in the reconstructed TDI counterparts. The levels are slightly below 0.001 as expected. The right panel shows how many attempts of Algorithm 1 were required before reaching the tolerance level.

There is no explicit requirement on the waveform f, but the assumption in (7) that a slowly oscillating part can be extracted from the waveform is critical for the approximations to be valid. Given the system of equations (13) governing the TDI counterparts, we see that parameters of at most three general signals (which in practice often degenerates into two) can be extracted. However, by imposing constraints on the waveform f the number of unknown parameters reduces for each GW. As an example, instead of estimating f at each time point, only the frequency and frequency derivative need to be extracted if it is assumed that the GW is emitted by a mildly chirping galactic binary. This enables the identification of several sources of gravitational waves with overlapping frequency content. Isolating data (*e.g.*, in narrow frequency bands) before estimating source parameters facilitates a deterministic approach for estimating parameters from a substantially larger number of sources across a wider frequency range.

Conclusions. – In this paper, we describe how to approximate the LISA response of a mildly chirping gravitational wave under the assumption that $|\beta_{j_1,j_2}(t)|$ is small by using tri-linear representations, and illustrate this by numerical examples. We briefly mention how the methodology can be generalized to approximate events with stronger chirp component.

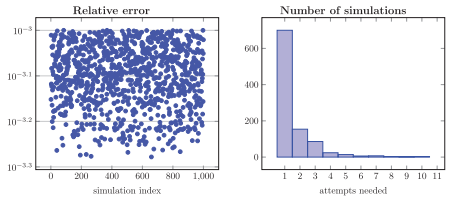

Fig. 3: Results from 1000 simulations of algorithm 1. Errors in the left panel, and a histogram over the number of attempts to reach tolerance level in the right panel.

Given fixed astrophysical objects, the tri-linear approximation allows for the separation of the geometric contributions of the spacecraft and information about the GW and its source. The latter decouples into the waveform $h^{\alpha}(t)$, the direction of propagation $\tilde{\mathsf{k}}$ and the matrix elements e. The dependency of the relative approximation error on ω_0^2, which holds for low frequencies, has been discussed and verified through numerical experiments. A simple algorithm for parameter estimation using this representation was constructed and applied to an example with isolated GWs. For this setup, it is not necessary to constraint the waveform f. However, in more complex scenarios where the data for instance contain noise or multiple GWs (overlapping in the same frequency band), problem-dependent constraints should be included in the estimation of f. Properties regarding convergence and sensitiviy to noise will depend strongly on the choice of constraints. However, while additional information such as knowledge about noise power spectral density will play an important role in the estimation procedure, the use of the tri-linear representation as a forward model will not be impacted.

Data availability statement: The data that support the findings of this study are available upon reasonable request from the authors.

REFERENCES

[1] Amaro Seoane P., Aoudia S., Audley H., Auger G., Babak S., Baker J., Barausse E., Barke S., Bassan M., Beckmann V. *et al.*, arXiv:1305.5720 (2013).
[2] Amaro-Seoane P., Audley H., Babak S., Baker J., Barausse E., Bender P., Berti E., Binetruy P., Born M., Bortoluzzi D. and Camp J., arXiv preprint, arXiv:1702.00786 (2017).
[3] Adams M. R., Cornish N. J. and Littenberg T. B., *Phys. Rev. D*, **86** (2012) 124032.
[4] Korol V., Rossi E. M. and Barausse E., *Mon. Not. R. Astron. Soc.*, **483** (2019) 5518.
[5] Burdge K. B., Coughlin M. W., Fuller J., Kupfer T., Bellm E. C., Bildsten L., Graham M. J., Kaplan D. L., Roestel J. V., Dekany R. G. and Duev D., *Nature*, **571** (2019) 528.
[6] Gair J., Hewitson M., Petiteau A. and Mueller G., arXiv preprint, arXiv:2201.10593 (2022).

[7] Benacquista M., *Lisa and the galactic population of compact binaries*, in *Handbook of Gravitational Wave Astronomy*, edited by Bamb C., Katsanevas S. and Kokkotas K. D. (Springer, Singapore) 2021, pp. 1–24.

[8] Abbott B. P., Abbott R., Abbott T., Abernathy M., Acernese F., Ackley K., Adams C., Adams T., Addesso P., Adhikari R. *et al.*, *Phys. Rev. Lett.*, **116** (2016) 061102.

[9] Abbott B. P., Abbott R., Abbott T. D., Abernathy M. R., Acernese F., Ackley K., Adams C., Adams T., Addesso P., Adhikari R. X. and Adya V. B., *Phys. Rev. Lett.*, **116** (2016) 241103.

[10] Abbott B. P., Abbott R., Abbott T. D., Acernese F., Ackley K., Adams C., Adams T., Addesso P., Adhikari R. X., Adya V. B. and Affeldt C., *Phys. Rev. Lett.*, **119** (2017) 141101.

[11] Abbott B. P., Abbott R., Abbott T. D., Acernese F., Ackley K., Adams C., Adams T., Addesso P., Adhikari R. X., Adya V. B. and Affeldt C., *Phys. Rev. Lett.*, **119** (2017) 161101.

[12] Abbott R., Abbott T. D., Abraham S., Acernese F., Ackley K., Adams C., Adhikari R. X., Adya V. B., Affeldt C., Agathos M. and Agatsuma K., *Phys. Rev. Lett.*, **125** (2020) 101102.

[13] Abbott R., Abbott T. D., Abraham S., Acernese F., Ackley K., Adams A., Adams C., Adhikari R. X., Adya V. B., Affeldt C. and Agarwal D., *Astrophys. J.*, **915** (2021) L5.

[14] Aasi J., Abbott B., Abbott R., Abbott T., Abernathy M., Ackley K., Adams C., Adams T., Addesso P., Adhikari R. *et al.*, *Class. Quantum Grav.*, **32** (2015) 074001.

[15] Acernese F. a., Agathos M., Agatsuma K., Aisa D., Allemandou N., Allocca A., Amarni J., Astone P., Balestri G., Ballardin G. *et al.*, *Class. Quantum Grav.*, **32** (2014) 024001.

[16] Aso Y., Michimura Y., Somiya K., Ando M., Miyakawa O., Sekiguchi T., Tatsumi D., Yamamoto H., Collaboration K. *et al.*, *Phys. Rev. D*, **88** (2013) 043007.

[17] Lück H., Team G. *et al.*, *Class. Quantum Grav.*, **14** (1997) 1471.

[18] Pitkin M., Reid S., Rowan S. and Hough J., *Living Rev. Relativ.*, **14** (2011) 1.

[19] Wanner G., *Nat. Phys.*, **15** (2019) 200.

[20] Cornish N. J. and Larson S. L., *Phys. Rev. D*, **67** (2003) 103001.

[21] Cornish N. J. and Crowder J., *Phys. Rev. D*, **72** (2005) 043005.

[22] Littenberg T. B., Cornish N. J., Lackeos K. and Robson T., *Phys. Rev. D*, **101** (2020) 123021.

[23] Cutler C. and Flanagan E. E., *Phys. Rev. D*, **49** (1994) 2658.

[24] Dhurandhar S. and Sathyaprakash B. S., *Phys. Rev. D*, **49** (1994) 1707.

[25] Poisson E. and Will C. M., *Phys. Rev. D*, **52** (1995) 848.

[26] Sathyaprakash B. S. and Dhurandhar S., *Phys. Rev. D*, **44** (1991) 3819.

[27] Hawking Stephen W. and Israel Werner, *Three Hundred Years of Gravitation* (Cambridge University Press) 1989.

[28] Brown D. A., Crowder J., Cutler C., Mandel I. and Vallisneri M., *Class. Quantum Grav.*, **24** (2007) S595.

[29] Cornish N., Sampson L., Yunes N. and Pretorius F., *Phys. Rev. D*, **84** (2011) 062003.

[30] Cornish N. J. and Littenberg T. B., *Phys. Rev. D*, **76** (2007) 083006.

[31] Crowder J. and Cornish N. J., *Phys. Rev. D*, **75** (2007) 043008.

[32] Gair J. R., Porter E., Babak S. and Barack L., *Class. Quantum Grav.*, **25** (2008) 184030.

[33] Littenberg T. B. and Cornish N. J., *Phys. Rev. D*, **80** (2009) 063007.

[34] Stroeer A. and Veitch J., *Phys. Rev. D*, **80** (2009) 064032.

[35] Trias M., Vecchio A. and Veitch J., *Class. Quantum Grav.*, **26** (2009) 204024.

[36] Umstätter R., Christensen N., Hendry M., Meyer R., Simha V., Veitch J., Vigeland S. and Woan G., *Phys. Rev. D*, **72** (2005) 022001.

[37] Van Der Sluys M., Raymond V., Mandel I., Röver C., Christensen N., Kalogera V., Meyer R. and Vecchio A., *Class. Quantum Grav.*, **25** (2008) 184011.

[38] Cornish N. J. and Rubbo L. J., *Phys. Rev. D*, **67** (2003) 022001.

[39] Vallisneri M., *Phys. Rev. D*, **71** (2005) 022001.

[40] Krolak A., Tinto M. and Vallisneri M., *Phys. Rev. D*, **70** (2004) 022003.

[41] Armstrong J., Estabrook F. and Tinto M., *Astrophys. J.*, **527** (1999) 814.

[42] Wahlquist H., *Gen. Relativ. Gravit.*, **19** (1987) 1101.

[43] Tinto M. and Dhurandhar S. V., *Living Rev. Relativ.*, **24** (2021) 1.

[44] Dhurandhar S., Joshi P. and Tinto M., *Phys. Rev. D*, **105** (2022) 084063.

[45] Tinto M. and Armstrong J. W., *Phys. Rev. D*, **59** (1999) 102003.

[46] Mallat S., *A Wavelet Tour of Signal Processing* (Elsevier) 1999.

[47] *Lisa data challenges*, last accessed 12 August 2022, `https://lisa-ldc.lal.in2p3.fr/`.

[48] Golub G. and Pereysa V., *Differentiation of pseudoinverses, separable nonlinear least square problems and other tales*, in *Generalized Inverses and Applications* (Elsevier) 1976, pp. 303–324.

[49] Comon P., Luciani X. and De Almeida A. L., *J. Chemom.: J. Chemom. Soc.*, **23** (2009) 393.

[50] Beylkin G. and Mohlenkamp M. J., *Proc. Natl. Acad. Sci. U.S.A.*, **99** (2002) 10246.

[51] Eriksson Anders and Van Den Hengel Anton, *Efficient computation of robust low-rank matrix approximations in the presence of missing data using the L1 norm*, in *2010 IEEE Computer Society Conference on Computer Vision and Pattern Recognition* (IEEE) 2010, pp. 771–778.

[52] Andersson F. and Carlsson M., *Constr. Approx.*, **38** (2013) 489.